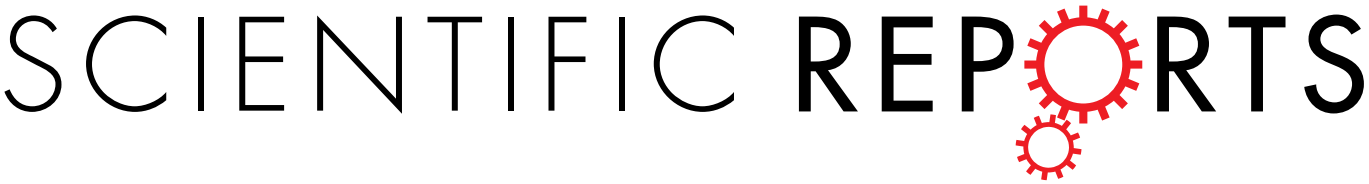

OPEN

Quantum Computation Based on Photons with Three Degrees of Freedom

Received: 15 December 2015
Accepted: 26 April 2016
Published: 13 May 2016

Ming-Xing Luo[1], Hui-Ran Li[1], Hong Lai[2] & Xiaojun Wang[3]

Quantum systems are important resources for quantum computer. Different from previous encoding forms using quantum systems with one degree of freedom (DoF) or two DoFs, we investigate the possibility of photon systems encoding with three DoFs consisting of the polarization DoF and two spatial DoFs. By exploring the optical circular birefringence induced by an NV center in a diamond embedded in the photonic crystal cavity, we propose several hybrid controlled-NOT (hybrid CNOT) gates operating on the two-photon or one-photon system. These hybrid CNOT gates show that three DoFs may be encoded as independent qubits without auxiliary DoFs. Our result provides a useful way to reduce quantum simulation resources by exploring complex quantum systems for quantum applications requiring large qubit systems.

Quantum computer has shown its superiority for solving difficult problems such as the large integer decomposition[1–3] and data searching[4,5]. Since its difficult the large integer decomposition is the mathematical foundation of the well-known RSA cryptography which may be used for classical cryptographic applications[6–8]. Most of these quantum computation tasks may be completed with evolutions of quantum systems and desired quantum measurements[1–5,9,10]. If the quantum circuit model[11] is applied, these evolutions may be synthesized by series of local quantum gates. Exactly, proper small gates such as the controlled phase-flip (CZ) gate or controlled-not (CNOT) gate combined with single-qubit gates[12–14] can be used to implement quantum tasks with multiple qubits. These small gates construct a universal quantum gate set for quantum computing. Up to now, the CNOT gate has been widely implemented using several quantum systems, such as the linear optics[15,16], ion trap[17,18], atom[19,20], and nuclear magnetic resonance[21,22].

The solid-state quantum system has also attracted much attentions in quantum simulations because of its special optical property and scalability[23–26]. Moreover, electron-spin qubits associated with the nitrogen-vacancy (NV) defect centers are particularly useful. In fact, due to the long room-temperature coherent time[27], the negatively charged NV defect center in the diamond lattice, consisting of a substitutional ^{14}N atom and an adjacent vacancy, is an attractive candidate for quantum information processing. It has been used to prepare and detect optical sources[28–33], generate hybrid quantum entanglements between the NV center and photon[34], or electrons[35,36], purify two-photonic hyperentanglement in both the polarization and spatial DoFs[37], or implement the CZ gate between the NV centers assisted by the microsphere cavity[38,39]. The single-electron and nuclear-spin states can be faithfully detected even under ambient conditions[40,41], when the electron spin of the NV defect center couples to nearby ^{13}C nuclear spins. Another diamond NV^- center is proposed with six electrons from the nitrogen and three carbons surrounding the vacancy[42], which is confined in a microtoroidal resonator (MTR)[43] with the quantized whispering-gallery mode (WGM). This useful system allows for an ultrahigh-Q and a small mode volume of WGM microresonators[44–46], which has been applied to construct quantum gates on electron-spin qubits[47,48] or remote qubits[49,50]. Furthermore, recent experiments have assembled several hybrid systems, where colour centers in diamond nanocrystals or bulk diamond are coupled to the evanescent fields of cavities, which are defined in non-diamond materials coupling to WGMs in a silica micro-sphere[50–52], diamond-GaP micro-disk[53], GaP micro-ring cavities[54], or SiN photonic crystal[55].

Most of previous quantum simulations focused on systems with single DoF[15–22] or hybrid systems[56–60]. A few schemes have considered photons with two DoFs[61,62]. Our recent result[63] presents the independence of two DoFs (polarization DoF and spatial DoF) of photonic system, and then is used to construct the ququart

[1]Information Security and National Computing Grid Laboratory, Southwest Jiaotong University, Chengdu 610031, China. [2]School of Computer and Information Science, Southwest University, Chongqing 400715, China. [3]School of Electronic Engineering, Dublin City University, Dublin 9, Ireland. Correspondence and requests for materials should be addressed to M.-X.L. (email: mxluo@home.swjtu.edu.cn)

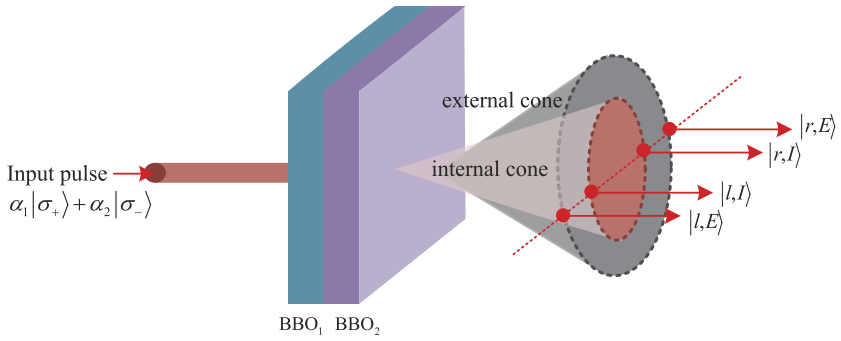

Figure 1. Schematic photon generation from the internal (*I*) and external (*E*) cone assisted by a two-crystal system. Polarized state as an input pulse passes through two 0.5 mm thick Type I β-barium-borate (BBO) crystal slabs. The input photon is created at a degenerate wavelength $\lambda = 2\lambda_p$ by each BBO crystal along two correlated directions belonging to the lateral surfaces of two SPDC cones, with full aperture angles θ_I and θ_E, respectively. The internal (*I*) and external (*E*) cone correspond to the first and the second crystal, respectively. The annular sections of each emission cone, with approximate diameters d_I and d_E are intercepted by a single eight-hole screen. The dichotomy existing between the *I* cone and *E* cone is identified as an independent DoF. The corresponding mode emission as $l(r)$ by referring to the left (right) side of each cone.

(four-dimensional) quantum logic[64]. Thus quantum simulation resources may be saved one half. In this paper, we further reduce quantum resources by considering photonic systems with three DoFs. Motivated by recent schemes[65,66], each photon may be encoded with two circularly polarized states and four modes, i.e., $|l, I\rangle$,$|r, I\rangle$ and $|l, E\rangle$,$|r, E\rangle$ for two crystal emissions. Here, $l(r)$ refers to the left (right) side of each cone and $I(E)$ denotes the internal (external) cone, as shown in Fig. 1. A general state is given by the product of one polarization state and two longitudinal momentum states. In the follow, we will investigate these photonic DoFs for the quantum simulation, without using auxiliary DoFs. From the quantum circuit model, CNOT gate will be schematically implemented on these DoFs of photonic states assisted by NV centers. For the symmetry of two spatial modes in each photonic system, fifteen CNOT gates are required to operate on the polarization DoFs and spatial-DoFs of the two-photon or one-photon system. Each gate is completed by interacting photons to auxiliary NV centers, disentangling NV centers, and correcting the emitting photons. These schemes are beyond to previous CNOT gates on the same DoF of two-photon state[14,15,56,57], hybrid CNOT gates on the photon and stationary electron spins in quantum dots[58–61], or different DoFs of two photons[62,63]. Our theoretical result shows that three DoFs of each photonic system can be used as independent qubits in one quantum task. Hence, two thirds of quantum resources may be saved for quantum simulations with large qubit systems, such as the Shor's algorithm.

Results

To show the encoding independence of the polarization DoF and two spatial DoFs of each photon, it is necessary to prove that all quantum transformations in $SU(2^n)$ may be implemented on these DoFs. Based on the theory of the universal logic gates[12–14], it is sufficient to consider the CNOT gate on any two DoFs of the photonic system. It means that fifteen CNOT gates should be performed on photonic systems with three DoFs, where nine CNOT gates are on the two-photon system (all combinations of three DoFs) and six CNOT gates are on the one photon system. By exploring optical selection rules of the NV center in the crystal cavity, these CNOT gates may be realized without altering DoFs and auxiliary DoFs during implementations. In this case, each photonic DoF can be encoded as an independent qubit in quantum applications.

Photon with three DoFs. Circularly polarized photon in the state $\alpha_1|L\rangle + \alpha_2|R\rangle$ (left circularly polarized state $|L\rangle$ and right circularly polarized state $|R\rangle$) is created at a degenerate wavelength $\lambda = 2\lambda_p$ by each BBO crystal along two correlated directions belonging to the lateral surfaces of two SPDC cones, with full aperture angles θ_I and θ_E, respectively[64,65], as shown in Fig. 1. The output state is dependent of these angles. *I* refers to the internal cone whereas *E* denotes the external cone, corresponding to the first and the second crystal, respectively. The dichotomy existing between the *I* cone and *E* cone is thus identified as an independent DoF, i.e., the corresponding mode emission as $l(r)$ by referring to the left (right) side of each cone[64,65]. If the pump coherence length exceeds more than one order of magnitude the total crystal length, the coherence and indistinguishability between two crystal emissions may be guaranteed[64,65]. Two conical emissions are then transformed into two cylindrical ones by a positive lens with focal length *f*, located at a distance *f* from the intermediate point of the second crystal device. By selecting four pairs of correlated modes with an eight-hole screen, $|l, I\rangle$ and $|r, I\rangle$ for the first crystal and $|l, E\rangle$ and $|r, E\rangle$ for the second crystal emission, a general photonic state is prepared as the product of one polarization state and two longitudinal momentum states (or, equivalently, a ququart state) and is expressed as a 3-qubit state:

$$|\phi\rangle = (\alpha_1|L\rangle + \alpha_2|R\rangle) \otimes (\beta_1|l, I\rangle + \beta_2|r, I\rangle + \beta_3|l, E\rangle + \beta_4|r, E\rangle) \quad (1)$$

where $|\alpha_1|^2 + |\alpha_2|^2 = 1$ and $|\beta_1|^2 + |\beta_2|^2 + |\beta_3|^2 + |\beta_4|^2 = 1$. Here, β_j are dependent of aperture angles θ_I and θ_E, and focal length *f*, which are not goals in this paper[64,65].

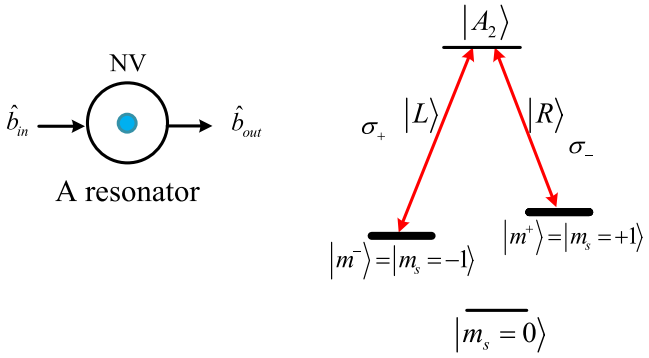

Figure 2. Schematic NV center coupling to the resonator and possible Λ-type optical transitions in the NV center. $\hat{a}_{in}$ and $\hat{a}_{out}$ are the input and output field operators of a waveguide, respectively. The bold levels encode qubits, i.e., $|m^{\pm}\rangle = |m_s = \pm\rangle$. The transition $|m^-\rangle \to |A_2\rangle$ is derived by a left circularly polarized photon σ_+ ($|L\rangle$), and $|m^+\rangle \to |A_2\rangle$ is derived by a right circularly polarized photon σ_- ($|R\rangle$).

A diamond NV center coupled to an MTR with a WGM. Schematic NV center in a diamond embedded in a photonic crystal cavity is shown in Fig. 2. The negatively charged NV center is consisted of a substitutional nitrogen atom and an adjacent vacancy with six electrons. The Λ-type three-level system is realized using specific excited state $|A_2\rangle = (|E_-\rangle|m^+\rangle + |E_+\rangle|m^-\rangle)$ as an ancillary state[66,34]. Here, $|E_\pm\rangle$ are orbital states with angular momentum projection along the NV axis. The ground state is an electronic spin triplet with a splitting of 2.88 GHz between the magnetic sublevels $|0\rangle(m_s = 0)$ and $|m^\pm\rangle(m_s = \pm 1)$[34]. $|A_2\rangle$ may decay into two ground states $|m^-\rangle$ and $|m^+\rangle$ by exciting the NV center with a polarized 2-ns p-pulse that is shorter than the emission timescale, and the reflection may be separated from fluorescence photons using detection timing[34]. The normal boundary condition $\hat{b}_{out} = \hat{b}_{in} + \sqrt{\kappa}\hat{a}$ is used to derive the optical selection rule with the input field $\hat{b}_{in}$, output field $\hat{b}_{out}$ and cavity field operator $\hat{a}$. If spins stay in the ground states most of the time[67], the optical reflection coefficient may be approximately defined in the follow (see Methods)

$$r(\omega) = \frac{\left(i\delta\omega_c - \frac{\kappa}{2} + \frac{\kappa_s}{2}\right)\left(i\delta\omega_e + \frac{\gamma}{2}\right) + g^2}{\left(i\delta\omega_c + \frac{\kappa}{2} + \frac{\kappa_s}{2}\right)\left(i\delta\omega_e + \frac{\gamma}{2}\right) + g^2} := |r(\omega)|e^{i\theta} \tag{2}$$

where $\delta\omega_c$ and $\delta\omega_e$ are frequency detunings satisfying $\delta\omega_c = \omega_c - \omega$ and $\delta\omega_e = \omega_e - \omega$. ω_c, ω and ω_e are the frequencies of the cavity mode, input photon pulse, and NV center, respectively. g is the coupling strength between the cavity and the NV center. κ, κ_s and γ are the damping rate of the cavity, cavity side leakage mode, and spontaneous decay rate of the NV center, respectively. If define the cooperativity $C = 2g^2/(\gamma\kappa)$, the photonic reflection probability[68] is determined by the cooperativity C and the cavity tuning as follow

$$P = 1 - \frac{1 + 4C + \left(\frac{\delta\omega_c}{\gamma}\right)^2}{1 + 4C + 4C^2 + \left(\frac{\delta\omega_c}{\gamma}\right)^2} \tag{3}$$

Considering the coupling strength $g = 0$, an NV center is uncoupled from the cavity (the cold cavity), and the reflection coefficient $r(\omega)$ becomes

$$r_0(\omega) = \frac{i\delta\omega_c - \frac{\kappa}{2} + \frac{\kappa_s}{2}}{i\delta\omega_c + \frac{\kappa}{2} + \frac{\kappa_s}{2}} =: |r_0(\omega)|e^{i\theta_0} \tag{4}$$

Thus the input pulse in the polarized state $|L\rangle$ gains a phase shift θ after reflecting from the hot cavity ($g > 0$) with the NV center $|m^-\rangle$, or a phase shift θ_0 after reflecting from the cold cavity ($g = 0$) with the NV center $|m^+\rangle$. The input pulse in the state $|R\rangle$ gains a phase shift θ_0 after reflecting from the cold cavity with the NV center $|m^-\rangle$, or a phase shift θ after reflecting from the hot cavity with the NV center $|m^+\rangle$. By choosing a proper frequency detuning $\delta\omega_e = 0$[66] and the cooperativity $C \gg 1$, the reflection coefficients may satisfy $|r(\omega)| \approx 1$ and $|r_0(\omega)| \approx 1$ when the cavity side leakage κ_s is negligible. By adjusting the frequencies ω and ω_c such that $\delta\omega_c/\kappa \to 0$ and $C \gg 1$, the phase shifts may be realized as $\theta = 0$ and $\theta_0 = \pi$. Hence, the following optical transition may be obtained as

$$\begin{aligned} &|R\rangle|m^-\rangle \to -|R\rangle|m^-\rangle,\ |R\rangle|m^+\rangle \to |R\rangle|m^+\rangle, \\ &|L\rangle|m^-\rangle \to |L\rangle|m^-\rangle,\ |L\rangle|m^+\rangle \to -|L\rangle|m^+\rangle. \end{aligned} \tag{5}$$

From this optical transition, an NV center requires a polarization-degenerate cavity mode, which is also suitable in H1 photonic crystals[69,70] and fiber-based cavities[71].

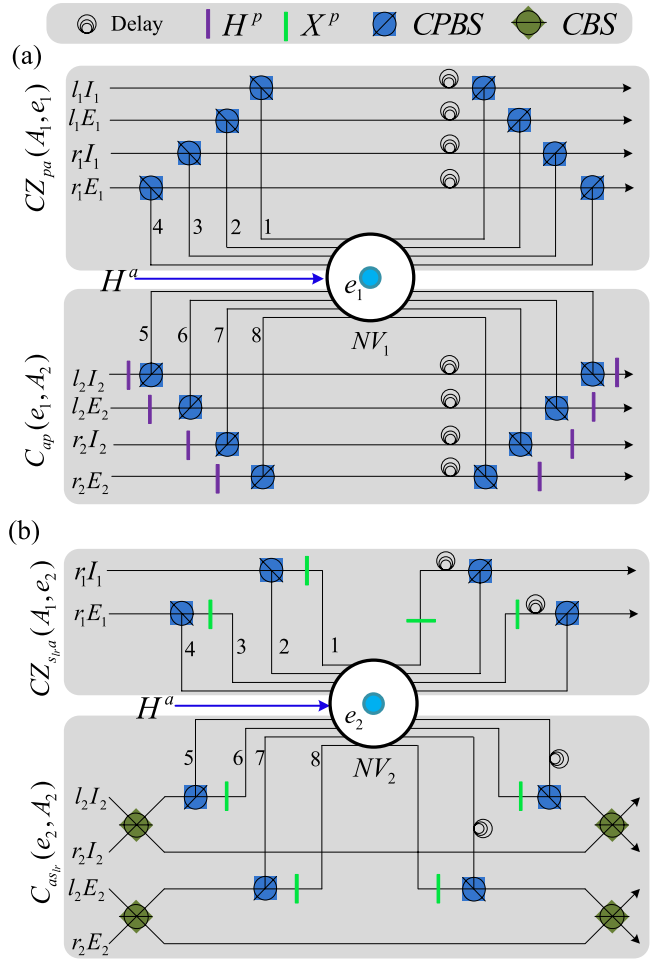

Figure 3. Schematic CNOT gate on the same DoF of two photons. (**a**) Schematic CNOT gate on the polarization DoFs of two photons. CPBS represents a polarizing beam splitter in the circular basis, which transmits $|R\rangle$ and reflects $|L\rangle$. CBS represents a 50% 50 beam splitter to perform the Hadamard operation on the spatial DoF of a photon. X represents a waveplate to implement the bit-flip operation $X^p = |R\rangle\langle L| + |L\rangle\langle R|$. H^a represents the Hadamard operation on the NV center in a cavity. (**b**) Schematic CNOT gate on the spatial DoFs of two photons. H^p represents a half-wave plate (HWP) to perform the Hadamard operation on the polarization DoF of a photon. The numbers 1, 2, …, 8 denote the orders for an input pulse to interact with an NV center.

CNOT gate on the same DoF of the two-photon system. Schematic CNOT gate on the same DoF of the two-photon system is shown in Fig. 3. NV centers e_i trapped in the photonic crystal NV_i are initially prepared in the superposition states $|+\rangle_{e_i} := (|m^-\rangle + |m^+\rangle)/\sqrt{2}$. Two input photons A_1 and A_2 are in the states $|\phi\rangle_{A_i} = (\alpha_{i1}|R\rangle + \alpha_{i2}|L\rangle) \otimes (\beta_{i1}|l_iI_i\rangle + \beta_{i2}|l_iE_i\rangle + \beta_{i3}|r_iI_i\rangle + \beta_{i4}|r_iE_i\rangle)$, $i = 1, 2$. Figure 3(a) is used to complete the CNOT gate on the polarization DoFs of two photons, i.e.,

$$C_{pp}(A_1, A_2) = |R\rangle\langle R| \otimes (|R\rangle\langle R| + |L\rangle\langle L|) + |L\rangle\langle L| \otimes (|R\rangle\langle L| + |L\rangle\langle R|) \tag{6}$$

In detail, the photon A_1 from each spatial mode (l_1I_1, l_1E_1, r_1I_1 or r_1E_1) evolves as $CPBS \rightarrow NV_1 \rightarrow CPBS$ to complete the following controlled phase gate

$$CZ_{pa}(A_1, e_1) = |R\rangle\langle R| \otimes (|m^-\rangle\langle m^-| + |m^+\rangle\langle m^+|) + |L\rangle\langle L| \otimes (|m^-\rangle\langle m^-| - |m^+\rangle\langle m^+|) \tag{7}$$

on the polarization DoF and the NV center e_1 (see Appendix A of Supplementary Information for details). And then, after one Hadamard operation H^a on the NV center e_1 in the NV_1, the photon A_2 from each spatial mode evolves as $H^p \rightarrow CPBS \rightarrow NV_1 \rightarrow CPBS \rightarrow H^p$ to complete the following hybrid CNOT gate

$$C_{ap}(e_1, A_2) = |m^-\rangle\langle m^-| \otimes (|R\rangle\langle R| + |L\rangle\langle L|) + |m^+\rangle\langle m^+| \otimes (|R\rangle\langle L| + |L\rangle\langle R|) \tag{8}$$

on the NV center e_1 and the polarization DoF of the photon A_2 (see Appendix A of Supplementary Information for details). Now, after disentangling the NV center e_1 using the measurement under the basis

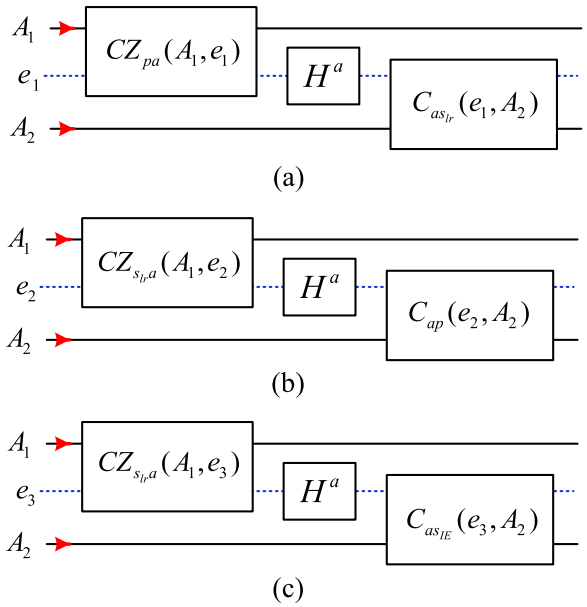

Figure 4. Schematic CNOT gate on different DoFs of the two-photon system. (**a**) Schematic CNOT gate on the polarization DoF of one photon and the spatial DoF $\{l, r\}$ of the other. (**b**) Schematic CNOT gate on the spatial DoF $\{l, r\}$ of one photon and the polarization DoF of the other. (**c**) Schematic CNOT gate on the spatial DoF $\{l, r\}$ of one photon and the spatial DoF $\{I, E\}$ of the other photon. e_i denote auxiliary NV centers in the NV-cavity NV_i, $i = 1, 2, 3$. The subcircuits H^a, CZ_{pa}, C_{ap}, CZ_{sa} and C_{as} are shown in the Fig. 3.

$\{|\pm\rangle := (|m^-\rangle \pm |m^+\rangle)/\sqrt{2}\}$, the phase flip $Z^p = |R\rangle\langle R| - |L\rangle\langle L|$ is performed on the photon A_1 from each mode for the measurement outcome $|-\rangle_{e_1}$. Thus the CNOT gate $C_{pp}(A_1, A_2)$ has been realized on the photons A_1 and A_2.

Figure 3(b) is a schematic circuit to complete the CNOT gate on the spatial DoF $\{l, r\}$s of two photons, i.e.,

$$C_{ss_{l,r}}(A_1, A_2) = |l\rangle\langle l| \otimes (|l\rangle\langle l| + |r\rangle\langle r|) + |r\rangle\langle r| \otimes (|l\rangle\langle r| + |r\rangle\langle l|) \tag{9}$$

Here, the photon A_1 from each spatial mode r_1I_1 or r_1E_1 evolves as $CPBS \rightarrow NV_2 \rightarrow (X \rightarrow NV_2 \rightarrow X) \rightarrow CPBS$ to complete the following controlled phase gate

$$CZ_{s_{l,r}a}(A_1, e_2) = |l\rangle\langle l| \otimes (|l\rangle\langle l| + |r\rangle\langle r|) + |r\rangle\langle r| \otimes (|l\rangle\langle l| - |r\rangle\langle r|) \tag{10}$$

on the spatial DoF $\{l, r\}$ and the NV center e_2 in the state $|+\rangle$ (see Appendix B of Supplementary Information for details). Now, after a Hadamard gate H^a performed on the NV center e_2 in the NV_2, the followed circuit $CBS \rightarrow CPBS \rightarrow NV_2 \rightarrow (X \rightarrow NV_2 \rightarrow X) \rightarrow CPBS \rightarrow CBS$ for each mode pair (l_2I_2, r_2I_2) or (l_2E_2, r_2E_2) is used to complete the hybrid CNOT gate on the NV center e_2 and the spatial DoF $\{l, r\}$ of the photon A_2 (see Supplementary Information for details), i.e.,

$$C_{as_{l,r}}(e_2, A_1) = |m^-\rangle\langle m^-| \otimes (|l\rangle\langle l| + |r\rangle\langle r|) + |m^+\rangle\langle m^+| \otimes (|l\rangle\langle r| + |r\rangle\langle l|) \tag{11}$$

Now, the CNOT gate $C_{ss_{l,r}}(A_1, A_2)$ may be realized by disentangling the NV center e_2 using the measurement under the basis $\{|\pm\rangle\}$, where Z^p is performed on the photon A_1 from each spatial mode r_1I_1 and r_1E_1 for the measurement outcome $|-\rangle_{e_2}$.

A similar CNOT gate

$$C_{ss_{I,E}}(A_1, A_2) = |I\rangle\langle I| \otimes (|I\rangle\langle I| + |E\rangle\langle E|) + |E\rangle\langle E| \otimes (|I\rangle\langle E| + |E\rangle\langle I|) \tag{12}$$

holds for the spatial DoF $\{I, E\}$s of two photons using an NV center e_3 trapped in the optical cavity NV_3 (see Appendix C of Supplementary Information for details).

Hybrid CNOT gate on the different DoFs of the two-photon system. Figure 4(a) is a schematic circuit to implement the CNOT gate on the polarization DoF of the photon A_1 and the spatial DoF $\{l, r\}$ of the photon A_2, i.e.,

$$C_{ps_{l,r}}(A_1, A_2) = |R\rangle\langle R| \otimes (|l\rangle\langle l| + |r\rangle\langle r|) + |L\rangle\langle L| \otimes (|l\rangle\langle r| + |r\rangle\langle l|) \tag{13}$$

In fact, similar to the Fig. 3(a), the first controlled phase flip $CZ_{pa}(A_1, e_1)$ in the equation (7) is used to change the photon A_1 and the NV center e_1 from $|\phi\rangle_{A_1}|+\rangle_{e_1}$ to $CZ_{pa}(A_1, e_1)(|\phi\rangle_{A_1}|+\rangle_{e_1})$. And then, after one Hadamard operation H^a performed on the NV center e_1 in the NV_1, the followed circuit $CBS \rightarrow CPBS \rightarrow NV_1 \rightarrow (X \rightarrow NV_1 \rightarrow$

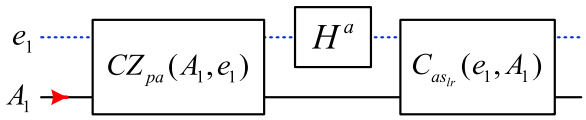

Figure 5. Hybrid CNOT gate on different DoFs of one photon. e_1 denotes an auxiliary NV center in the NV-cavity NV_1. The subcircuits CZ_{pa} and C_{as} are shown in the Fig. 3.

$X) \rightarrow CPBS \rightarrow CBS$ for each spatial mode pair (l_2I_2, r_2I_2) or (l_2E_2, r_2E_2) is used to complete the CNOT gate $C_{as}(e_2, A_1)$ in the equation (11) on the NV center e_1 and the spatial mode $\{l, r\}$ of the photon A_2 (similar to the Fig. 3(b)). After disentangling the NV center e_1 using the measurement under the basis $\{|\pm\rangle\}$, the hybrid CNOT gate $C_{ps_{l,r}}(A_1, A_2)$ is realized on the photons A_1 and A_2, where Z^p is performed on the photon A_1 from each spatial mode r_1I_1 and r_1E_1 for the measurement outcome $|-\rangle_{e_1}$, see Appendix D of Supplementary Information for details.

Similarly, after the controlled-phase flip $CZ_{pa}(A_1, e_1')$ on the photon A_1 and the NV center $e_{1'}$ in the state $|+\rangle$, a schematic circuit is applied to the photon A_2 from two spatial mode pairs (l_2I_2, l_2E_2) and (r_2I_2, r_2E_2) to complete the CNOT gate on the NV center $e_{1'}$ and the spatial DoF $\{I, E\}$ of the photon A_2 (see Appendix E of Supplementary Information for details). The hybrid CNOT gate

$$C_{ps_{I,E}}(A_1, A_2) = |R\rangle\langle R| \otimes (|I\rangle\langle I| + |E\rangle\langle E|) + |L\rangle\langle L| \otimes (|I\rangle\langle E| + |E\rangle\langle I|) \tag{14}$$

is implemented on the polarization DoF of the photon A_1 and the spatial DoF $\{I, E\}$ of the photon A_2 after disentangling the NV center $e_{1'}$.

Figure 4(b) is used to implement the CNOT gate on the spatial DoF $\{l, r\}$ of the photon A_1 and the polarization DoF of the photon A_2, i.e.,

$$C_{s_{l,r}p}(A_1, A_2) = |l\rangle\langle l| \otimes (|R\rangle\langle R| + |L\rangle\langle L|) + |r\rangle\langle r| \otimes (|R\rangle\langle L| + |L\rangle\langle R|) \tag{15}$$

In fact, similar to the evolutions as shown in the Fig. 3(b), the controlled phase gate $CZ_{s_{l,r}a}(A_1, e_2)$ in the equation (10) is performed on the photon A and the NV center e_2 in the state $|+\rangle$ to get $CS_{sa}(A_1, e_2)(|\phi\rangle_{A_1}|+\rangle_{e_2})$. And then, after one Hadamard operation H^a on the NV center e_2 in the NV_2, the followed circuit for the photon A_2 from each spatial mode is used to complete the CNOT gate $C_{ap}(e_2, A_2)$ on the NV center e_2 and the polarization DoF of the photon A_2 (see the Fig. 3(a)). The final joint state is $C_{ap}(e_2, A_2)CS_{s_{l,r}a}(A_1, e_2)(|\phi\rangle_{A_1}|\phi\rangle_{A_2})$. Finally, by disentangling the NV center e_2 using the measurement under the basis $\{|\pm\rangle\}$, the hybrid CNOT gate $C_{s_{l,r}p}(A_1, A_2)$ is realized, where $-I^p$ will be performed on the photon A_1 from each spatial mode r_1I_1 and r_1E_1 for the measurement outcome $|-\rangle_{e_2}$, see Appendix F of Supplementary Information for details. Moreover, if the second part of the present circuit above is applied to the photon A_1 from two spatial modes l_1I_1 and l_1E_1, the CNOT gate is implemented on the spatial DoF $\{I, E\}$ of the photon A_1 and the polarization DoF of the photon A_2, see Appendix G of Supplementary Information for details.

Figure 4(c) is used to implement the CNOT gate on the spatial DoF $\{l, r\}$ of the photon A_1 and the spatial DoF $\{I, E\}$ of the photon A_2, i.e,

$$C_{s_{l,r}s_{I,E}}(A_1, A_2) = |l\rangle\langle l| \otimes (|I\rangle\langle I| + |E\rangle\langle E|) + |r\rangle\langle r| \otimes (|I\rangle\langle E| + |E\rangle\langle I|) \tag{16}$$

In detail, similar to the evolutions as shown in the Fig. 3(b), the controlled phase gate $CZ_{s_{l,r}a}$ in the equation (10) is performed for the photon A and the NV center e_3 in the state $|+\rangle$ to get $CZ_{s_{l,r}a}(A_1, e_3)(|\phi\rangle_{A_1}|+\rangle_{e_3})$. And then, after one Hadamard operation H^a on the NV center e_3, the followed circuit for the photon A_2 from each spatial mode is used to realized the CNOT gate $C_{as_{I,E}}(e_3, A_2) = |m^-\rangle\langle m^-| \otimes (|I\rangle\langle I| + |E\rangle\langle E|) + |m^+\rangle\langle m^+| \otimes (|I\rangle\langle E| + |E\rangle\langle I|)$ on the NV center e_3 and the spatial DoF $\{I, E\}$ of the photon A_2. The final joint state is $C_{as_{I,E}}(e_3, A_2)CZ_{s_{l,r}a}(A_1, e_3)(|\phi\rangle_{A_1}|+\rangle_{e_3}|\phi\rangle_{A_2})$. Now, by disentangling the NV center e_3 using the measurement under the basis $\{|\pm\rangle\}$, $C_{s_{l,r}s_{I,E}}(A_1, A_2)$ may be deterministically realized, where $-I^p$ will be performed on the photon A_1 from each spatial mode l_1E_1 and r_1E_1 for the measurement outcome $|-\rangle_{e_3}$, see Appendix H of Supplementary Information for details. Similarly, the CNOT gate may be implemented on the spatial DoF $\{I, E\}$ of the photon A_1 and the spatial DoF $\{l, r\}$ of the photon A_2, see Appendix I of Supplementary Information for details.

Hybrid CNOT gate on different DoFs of one photon. Figure 5 is a schematic circuit to implement the CNOT gate $C_{ps_{l,r}}$ in the equation (13) on the polarization DoF and the spatial DoF $\{l, r\}$ of the photon A_1. In detail, similar to the Fig. 3(a), the controlled-phase flip CZ_{pa} in the equation (7) is used to change the photon A_1 and the NV center e_1 from $|\phi\rangle_{A_1}|+\rangle_{e_1}$ to $CZ_{pa}(A_1, e_1)(|\phi\rangle_{A_1}|+\rangle_{e_1})$. And then, after one Hadamard operation H^a performed on the NV center e_1, the followed CNOT gate C_{asl} in the equation (11) is performed on the NV center e_1 and the spatial DoF $\{l, r\}$ of the photon A_1 (similar to the Fig. 3(b)). After disentangling the NV center e_1 using the measurement under the basis $\{|\pm\rangle\}$, the hybrid CNOT gate $C_{ps_{l,r}}$ is realized on the photon A_1, where Z^p will be performed for the photon A_1 from each mode for the measurement outcome $|-\rangle_{e_1}$, see Appendix J of Supplementary

Information for details. Moreover, if the CNOT gate $C_{as_{IE}}(e_1, A_1)$ is performed on the NV center e_1 and the photon A_1 after $CZ_{pa}(A_1, e_1)$, the hybrid CNOT gate $C_{ps_{I,E}}$ in the equation (14) is realized on the photon A_1 after properly disentangling the auxiliary NV center, see Appendix K of Supplementary Information for details.

For the hybrid CNOT gate on the spatial DoF $\{l, r\}$ and the spatial DoF $\{I, E\}$ of the photon A_1, the photon A_1 from the spatial modes r_1I_1 and r_1E_1 passes through CBS, $-I$, CBS, sequentially. The photon A_1 evolves as follows

$$
\begin{aligned}
|\phi_1\rangle_{A_1} \xrightarrow[\text{mode pairs } (r_1I_1,\, r_1E_1)]{CBS} & \alpha_0|R\rangle|l_1I_1\rangle + \alpha_1|R\rangle|l_1E_1\rangle + \alpha_4|L\rangle|l_1I_1\rangle + \alpha_5|L\rangle|l_1E_1\rangle \\
& +\alpha_2'|R\rangle|r_1I_1\rangle + \alpha_3'|R\rangle|r_1E_1\rangle + \alpha_6'|L\rangle|r_1I_1\rangle + \alpha_7'|L\rangle|r_1E_1\rangle \\
\xrightarrow[\text{mode } r_1E_1]{-I} & \alpha_0|R\rangle|l_1I_1\rangle + \alpha_1|R\rangle|l_1E_1\rangle + \alpha_4|L\rangle|l_1I_1\rangle + \alpha_5|L\rangle|l_1E_1\rangle \\
& +\alpha_2'|R\rangle|r_1I_1\rangle - \alpha_3'|R\rangle|r_1E_1\rangle + \alpha_6'|L\rangle|r_1I_1\rangle - \alpha_7'|L\rangle|r_1E_1\rangle \\
\xrightarrow[\text{mode pairs } (r_1I_1,\, r_1E_1)]{CBS} & \alpha_0|R\rangle|l_1I_1\rangle + \alpha_1|R\rangle|l_1E_1\rangle + \alpha_4|L\rangle|l_1I_1\rangle + \alpha_5|L\rangle|l_1E_1\rangle \\
& +\alpha_3|R\rangle|r_1I_1\rangle + \alpha_2|R\rangle|r_1E_1\rangle + \alpha_7|L\rangle|r_1I_1\rangle + \alpha_6|L\rangle|r_1E_1\rangle
\end{aligned}
\tag{17}
$$

where $\alpha_2' = (\alpha_2' + \alpha_3')/\sqrt{2}, \alpha_3' = (\alpha_2' - \alpha_3')/\sqrt{2}, \alpha_6' = (\alpha_6' + \alpha_7')/\sqrt{2}$, and $\alpha_7' = (\alpha_6' - \alpha_7')/\sqrt{2}$. Similar circuit may be used to realize the hybrid CNOT gate on the spatial DoF $\{I, E\}$ and the spatial DoF $\{l, r\}$ of the photon A_1, see Appendix K of Supplementary Information for details. Moreover, the CNOT gates on the spatial mode DoF and the polarization DoF of the photon A_1 are easily realized by two flip waveplates on two spatial modes r_1I_1 and r_1E_1, or l_1E_1 and r_1E_1, respectively.

Discussions

In ideal conditions, one may neglect the cavity side leakage, and the reflection coefficients satisfy $|r_0(\omega)| \approx 1$ and $|r(\omega)| \approx 1$. The corresponding fidelities of the present CNOT gates are nearly 100%. In experiment, the general fidelity is defined by $F = \int |\langle\Phi|\rho_f|\Phi\rangle|$, where $|\Phi\rangle$ is the ideal final state without side leakage while ρ_f is the final state under a real situation with side leakage. In the resonant condition $\delta\omega_e = 0$, if the cavity side leakage is considered, the optical selection rule for the NV-cavity system given by the equation (5) becomes

$$
\begin{aligned}
&|R\rangle|m^-\rangle \rightarrow -|r_0||R\rangle|m^-\rangle,\ |R\rangle|m^+\rangle \rightarrow |r||R\rangle|m^+\rangle, \\
&|L\rangle|m^-\rangle \rightarrow |r||L\rangle|m^-\rangle,\ |L\rangle|m^+\rangle \rightarrow -|r_0||L\rangle|m^+\rangle.
\end{aligned}
\tag{18}
$$

Due to the exchangeability of two spatial DoFs of one photon with respect to random initial photons, the fidelities and efficiencies are evaluated for four CNOT gates: CNOT gate on two polarization DoFs, CNOT gate on two spatial DoFs, CNOT gate on the polarization DoF of one photon and the spatial DoF of the other photon, and CNOT gate on the polarization and spatial DoFs of one photon system, as shown in Figs 6 and 7, respectively. Generally, large cooperativity C and low relative detuning $\delta\omega_c/\kappa$ are required for high fidelities and efficiencies. For the diamond NV centers, the photoluminescence is partially unpolarized, and the emission with ZPL is only 4% of the total emission. ZPL with zero phonon line is only 4% of $\gamma = 2 \times 15\,\text{MHz}$[31]. For the diamond NV center in a MTR with WGM mode system, $|r(\omega)| \approx 0.95$ when $C \geq 18$[34] with small detuning $\delta\omega_c/\kappa \approx 0$; $|r(\omega)| \approx 1$ when $C \geq 50$ with small detuning $\delta\omega_c/\kappa \approx 0$ for $\kappa \approx 1\,\text{GHz}$ or $\kappa \approx 10\,\text{GHz}$. For our CNOT gates, if $C \geq 18$ and $\delta\omega_c/\kappa \approx 0.1$, their fidelities are greater than 82.6% and their efficiencies are greater than 75.4%. If $C \geq 50$ and $\delta\omega_c/\kappa \approx 0.1$, their fidelities are greater than 98.4% and their efficiencies are greater than 94.7%.

In conclusion, we have investigated the possibility of quantum simulations using photon systems with three DoFs. We have constructed fifteen schematic CNOT gates operating on the spatial and polarization DoFs of the two-photon system or one-photon system. Different from previous CNOT gate on the same DoF of the two-photon system[14,15,56,57], our schemes are based on different DoFs of two photons or one photon. Compared with hybrid implementations on the photon and stationary electron spins in quantum dots[58–61], the present CNOT circuits are ultimately realized on the photon system, and the electron spins in NV center are auxiliary resources to build the correlation between photons. The present schemes have shown that two different spatial DoFs may be viewed as independent qubits simultaneously, which has beyond previous independence of the polarization and spatial DoFs[62,63]. Although different DoFs may be easily exchanged in terms of encoding, the schematic operations are inconvenient for photon systems with two different spatial DoFs. The main reason is that the hybrid CNOT gates are not realized in one-shot manners. Thus, it is difficult to exchange these DoFs during applications, where different DoFs may be used as different encoding types such as the quantum Shor algorithm or the quantum search algorithm. Hence, our results are distinct from all previous quantum logic gates on different photons[14,15,56,57]. Our theoretical schemes have shown that three DoFs of photon systems may be independent in quantum information processing. Two thirds of the quantum resources may be saved in quantum simulations. With the recent experiments of the NV-cavity system[33–35], our schemes are expected to be applicable for the entanglement distribution or large-scale quantum computation.

Methods

A diamond NV center coupled to an MTR with a WGM. The master equation of the whole system may be expressed by a Lindblad form as follows

$$
\dot{\rho} = i\hbar[\rho, H] + \mathcal{H}_1\rho + \mathcal{H}_2\rho, \tag{19}
$$

where $H = H_1 + H_2 + H_3 + H_4$. $H_1 = \omega\hat{b}^\dagger\hat{b}$ is the Hamiltonian of an input photon pulse. $H_2 = g(\hat{a}\sigma_+ + \hat{a}^\dagger\sigma_-)$ is the standard Jaynes-Cummings Hamiltonian for a two-level system interacting with a single electromagnetic

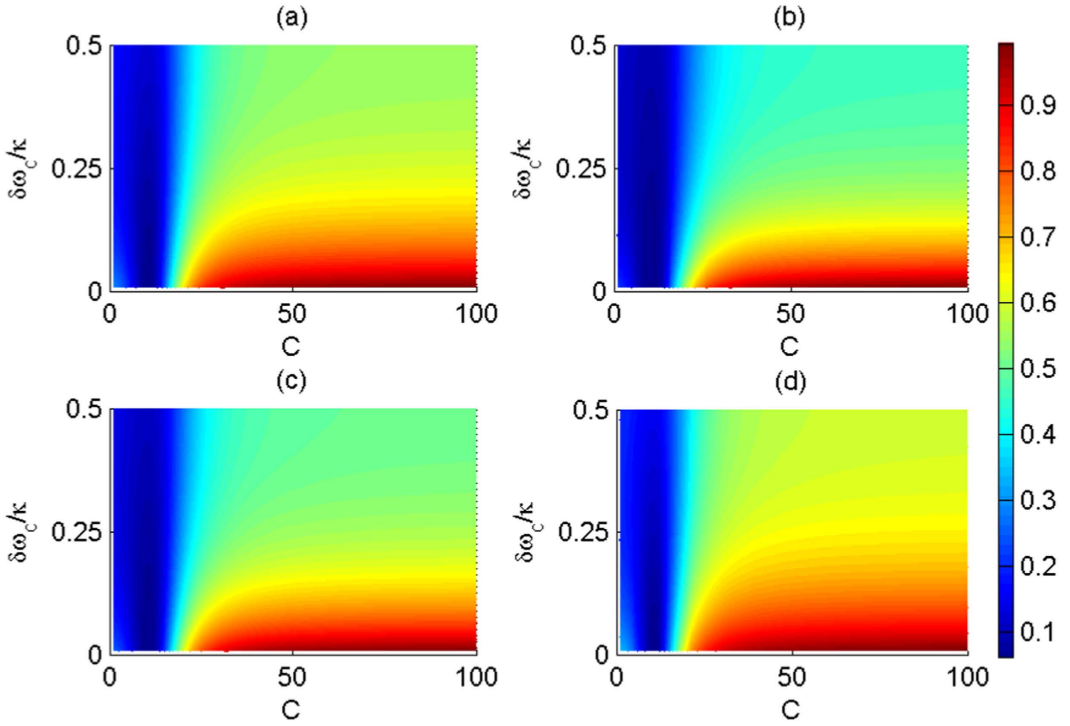

Figure 6. Average fidelities of the present CNOT gates vias the cooperativity C and relative detuning $\delta\omega_c/\kappa$. (**a**) The average fidelity of the CNOT gate on the polarization DoFs of two photons; (**b**) The average fidelity of the CNOT gate on the spatial DoFs of two photons; (**c**) The average fidelity of the hybrid CNOT gate on the polarization and spatial DoFs of the two-photon system; (**d**) The average fidelity of the hybrid CNOT gate on the polarization and spatial DoFs of the one photon system. The average fidelity is computed as the expectation of random input photons.

mode by applying the rotating wave approximation and dropping the energy nonconserving terms. σ_- and σ_+ are the Pauli raising and lowering operators, respectively. g is the coupling strength between the cavity and X^-. $H_3 = \frac{\omega_c}{2}\sigma_z$ is the Hamiltonian of the dipole. σ_z is the Pauli operator for the population inversion. $H_4 = \sqrt{\kappa}(\hat{a}^\dagger \hat{b}_{in} - \hat{a}\hat{b}_{in}^\dagger)$ is the interaction between the excitation field and system. $\mathcal{H}_1\rho = -\frac{\kappa+\kappa_s}{2}(\hat{b}^\dagger\hat{b}\rho + \rho\hat{b}^\dagger\hat{b} - 2\hat{b}\rho\hat{b}^\dagger)$ accounts for the damping of the input photon pulse. $\mathcal{H}_2\rho = \frac{\gamma}{2}(2\sigma_-\rho\sigma_+ - \sigma_+\sigma_-\rho - \rho\sigma_+\sigma_-)$ accounts for spontaneous emission of the dipole. The input-output optical relation of the NV center system may be calculated from the Heisenberg equations[67] in terms of the cavity field operator $\hat{a}$, input pulse field $\hat{b}$ and dipole operator σ_-,

$$\begin{aligned}\frac{d\hat{a}}{dt} &= -\left(i\delta\omega_c + \frac{\kappa}{2} + \frac{\kappa_s}{2}\right)\hat{a} - g\hat{\sigma}_- - \sqrt{\kappa}\hat{b}_{in},\\ \frac{d\sigma_-}{dt} &= -\left(i\delta\omega_e + \frac{\gamma}{2}\right)\hat{\sigma}_- - g\sigma_z\hat{a} + \sqrt{\gamma}\hat{b}_{in},\end{aligned} \tag{20}$$

If spins stay in the ground states most of the time [$\langle\sigma_-\rangle = -1$], the cavity output $\hat{b}_{out}$ is connected with the input field by the standard input-output relation by a reflection coefficient $r(\omega)$.

Measurement of the NV center e in cavity. To measure the NV center e of an entangled system $\alpha|m^-\rangle_e|\Omega_1\rangle + \beta|m^+\rangle_e|\Omega_2\rangle$, an auxiliary photon c in the state $\frac{1}{\sqrt{2}}(|R\rangle + |L\rangle)$ may be used as follows. Let the photon c pass through one CPBS to split the circular polarizations $|R\rangle$ and $|L\rangle$, and the right-circular polarization $|R\rangle$ interact with the cavity system, and its output combine with $|L\rangle$ of the photon c using the other CPBS. Thus, the joint system evolves

$$\begin{aligned}&\frac{\alpha}{\sqrt{2}}(|R\rangle + |L\rangle)_c|m^-\rangle_e|\Omega_1\rangle + \frac{\beta}{\sqrt{2}}(|R\rangle + |L\rangle)_c|m^+\rangle_e|\Omega_2\rangle\\ &\quad\mapsto \frac{\alpha}{\sqrt{2}}(|R\rangle - |L\rangle)_c|m^-\rangle_e|\Omega_1\rangle + \frac{\beta}{\sqrt{2}}(|R\rangle + |L\rangle)_c|m^+\rangle_e|\Omega_2\rangle.\end{aligned} \tag{21}$$

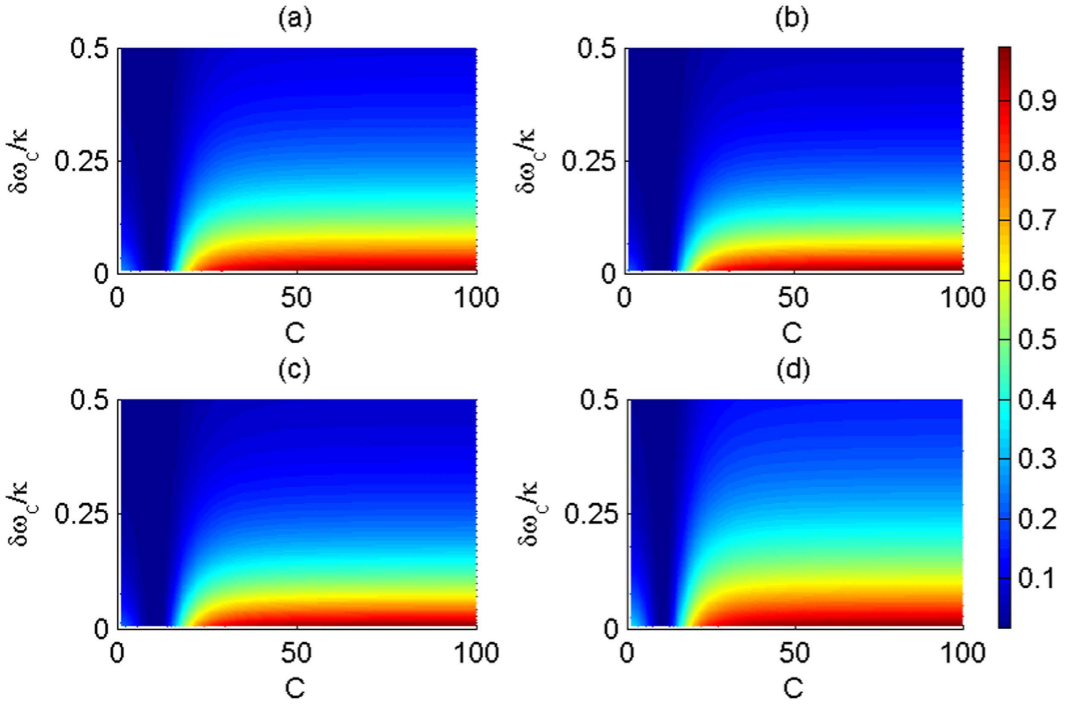

Figure 7. Average efficiencies of the present CNOT gates vias the cooperativity *C* and relative detuning $\delta\omega_c/\kappa$. (**a**) The average fidelity of the CNOT gate on the polarization DoFs of two photons; (**b**) The average fidelity of the CNOT gate on the spatial DoFs of two photons; (**c**) The average fidelity of the hybrid CNOT gate on the polarization and spatial DoFs of the two-photon system; (**d**) The average fidelity of the hybrid CNOT gate on the polarization and spatial DoFs of the one photon system. The average fidelity is computed as the expectation of random input photons.

Hence, the NV center *e* can be determined by measuring the photon in the orthogonal basis $\left\{\frac{1}{\sqrt{2}}(|R\rangle \pm |L\rangle)\right\}$. The NV center is $|m^-\rangle$ or $|m^+\rangle$ for the measurement outcome $\frac{1}{\sqrt{2}}(|R\rangle + |L\rangle)$ or $\frac{1}{\sqrt{2}}(|R\rangle - |L\rangle)$, respectively.

References

1. Nielsen, M. A. & Chuang, I. L. (ed.) [*Quantum Computation and Quantum Information*] [216–271] (Cambridge University Press, Cambridge, 2000).
2. Shor, P. W. Polynomial-time algorithms for prime factorization and discrete logarithms on a quantum computer. *SIAM J. Comput.* **26,** 1484–1509 (1997).
3. Li, J., Peng, X., Du, J. F. & Suter, D. An efficient exact quantum algorithm for the integer square-free decomposition problem. *Sci. Rep*. **2,** 260 (2012).
4. Grover, L. K. Quantum mechanics helps in searching for a needle in a haystack. *Phys. Rev. Lett.* **79,** 325–328 (1997).
5. Farhi, E. *et al.* A quantum adiabatic evolution algorithm applied to random instances of an NP-Complete problem. *Science* **292,** 472–475 (2001).
6. Li, B., Yu, Z.-H. & Fei, S.-M. Geometry of quantum computation with qutrits. *Sci. Rep*. **3,** 2594 (2013).
7. Guo, P., Wang, J., Geng, X. H., Kim, C. S. & Kim, J. U. A variable threshold-value authentication architecture for wireless mesh networks. *J Internet Tech*. **15,** 929–936 (2014).
8. Fu, Z., Sun, X., Liu, Q., Zhou, L. & Shu, J. Achieving efficient cloud search services: multi-keyword ranked search over encrypted cloud data supporting parallel computing. *IEICE Trans. Commun.* **98,** 190–200 (2015).
9. Li, J., Li, X., Yang, B. & Sun, X. Segmentation-based image copy-move forgery detection scheme. *IEEE Trans. Inf. Forensics Security* **10,** 507–518 (2015).
10. Luo, M.-X., Chen, X.-B., Yang Y.-X. & Wang, X. Geometry of quantum computation with qudits. *Sci. Rep*. **4,** 4044 (2014).
11. Deutsch, D. Quantum computational networks. *Proc. R. Soc. Lond. A* **425,** 73–90 (1989).
12. Barenco, A. *et al.* Elementary gates for quantum computation. *Phys. Rev. A* **52,** 3457–4467 (1995).
13. Sleator, T. & Weinfurter, H. Realizable universal quantum logic Gates. *Phys. Rev. Lett.* **74,** 4087–4090 (1995).
14. Shende, V., Bullock, S. S. & Markov, I. L. Synthesis of quantum-logic circuits. *IEEE Tran. Comput. AID Design* **26,** 1000–1010 (2006).
15. Knill, E., Laflamme, R. & Milburn, G. J. A scheme for efficient quantum computation with linear optics. *Nature* **409,** 46–52 (2001).
16. Nemoto, K. & Munro, W. J. Nearly deterministic linear optical controlled-NOT gate. *Phys. Rev. Lett.* **93,** 250502 (2004).
17. Cirac, J. I. & Zoller, P. Quantum computations with cold Trapped Ions. *Phys. Rev. Lett.* **74,** 4091 (1995).
18. Riebe, M. *et al.* Process tomography of Ion Trap quantum gates. *Phys. Rev. Lett.* **97,** 220407 (2006).
19. Monroe, C., Meekhof, D. M., King, B. E., Itano, W. M. & Wineland, D. J. Demonstration of a fundamental quantum logic gate, *Phys. Rev. Lett.* **75,** 4714 (1995).
20. Isenhower, L. *et al.* Demonstration of a neutral atom controlled-NOT quantum gate. *Phys. Rev. Lett.* **104,** 010503 (2010).
21. Vandersypen, L. M. *et al.* Experimental realization of Shor's quantum factoring algorithm using nuclear magnetic resonance. *Nature* **414,** 883–887 (2001).
22. Jones, J. A., Vedral, V., Ekert, A. & Castagnoli, G. Geometric quantum computation using nuclear magnetic resonance. *Nature* **403,** 869–871 (2000).
23. Li, X. *et al.* An all-optical quantum gate in a semiconductor quantum dot. *Science* **301,** 809–811 (2003).

24. Romero, G., Ballester, D., Wang, Y. M., Scarani, V. & Solano, E. Ultrafast quantum gates in circuit QED. *Phys. Rev. Lett.* **108,** 120501 (2012).
25. Stojanović, V. M., Fedorov, A., Wallraff, A. & Bruder, C. Quantum-control approach to realizing a Toffoli gate in circuit QED. *Phys. Rev. B* **85,** 054504 (2012).
26. Yamamoto, T., Pashkin, Y. A., Astafiev, O., Nakamura, Y. & Tsai, J. S. Demonstration of conditional gate operation using superconducting charge qubits. *Nature* **425,** 941–944 (2003).
27. Balasubramanian, G. *et al.* Ultralong spin coherence time in isotopically engineered diamond. *Nature Mater*. **8,** 383–387 (2009).
28. Charnock, F. T. & Kennedy, T. A. Combined optical and microwave approach for performing quantum spin operations on the nitrogen-vacancy center in diamond. *Phys. Rev. B* **64,** 041201 (2001).
29. Jelezko, F., Gaebel, T., Popa, I., Gruber, A. & Wrachtrup, J. Observation of coherent oscillations in a single electron spin. *Phys. Rev. Lett*. **92,** 076401 (2004).
30. Epstein, R. J., Mendoza, F. M., Kato, Y. K. & Awschalom, D. D. Anisotropic interactions of a single spin and dark-spin spectroscopy in diamond. *Nature Phys*. **1,** 94–98 (2005).
31. Gaebel, T. *et al.* Room-temperature coherent coupling of single spins in diamond. *Nature Phys*. **2,** 408–413 (2006).
32. Hanson, R., Mendoza, F. M., Epstein, R. J. & Awschalom, D. D. Polarization and readout of coupled single spins in diamond. *Phys. Rev. Lett.* **97,** 087601 (2006).
33. Fuchs, G. D., Dobrovitski, V. V., Toyli, D. M., Heremans, F. J. & Awschalom, D. D. Gigahertz dynamics of a strongly driven single quantum spin. *Science* **326,** 1520–1522 (2009).
34. Togan, E. *et al.* Quantum entanglement between an optical photon and a solid-state spin qubit. *Nature* **466,** 730–735 (2010).
35. Neumann, P. *et al.* Quantum register based on coupled electron spins in a room-temperature solid. *Nature Phys*. **6,** 249–253 (2010).
36. Zheng, A. S., Li, J. H., Yu, R., Lü, X. Y. & Wu, Y. Generation of Greenberger-Horne-Zeilinger state of distant diamond nitrogen-vacancy centers via nanocavity input-output process. *Opt. Express* **20,** 16902–16912 (2012).
37. Ren, B. C. & Deng, F. G. Hyperentanglement purification and concentration assisted by diamond NV centers inside photonic crystal cavities. *Laser Phys. Lett.* **10,** 115201 (2013).
38. Jelezko, F. *et al.* Observation of coherent oscillation of a single nuclear spin and realization of a two-qubit conditional quantum gate. *Phys. Rev. Lett.* **93,** 130501 (2004).
39. Yang, W. L., Yin, Z. Q., Xu, Z. Y., Feng, M. & Du, J. F. One-step implementation of multiqubit conditional phase gating with nitrogen-vacancy centers coupled to a high-Q silica microsphere cavity. *Appl. Phys. Lett*. **96,** 241113 (2010).
40. Yang, W. L., Xu, Z. Y., Feng, M. & Du, J. F. Entanglement of separate nitrogen-vacancy centers coupled to a whispering-gallery mode cavity. *New J. Phys.* **12,** 113039 (2010).
41. Dayan, B. *et al.* A photon turnstile dynamically regulated by one atom. *Science* **319,** 1062–1065 (2008).
42. Spillane, S. M. *et al.* Ultrahigh-Q toroidal microresonators for cavity quantum electrodynamics. *Phys. Rev. A* **71,** 013817 (2005).
43. Louyer, Y., Meschede, D. & Rauschenbeutel, A. Tunable whispering-gallery-mode resonators for cavity quantum electrodynamics. *Phys. Rev. A* **72,** 031801 (2005).
44. Vahala, K. J. Optical microcavities. *Nature* **424,** 839–846 (2003).
45. Wei, H.-R. & Deng, F.-G. Compact quantum gates on electron-spin qubits assisted by diamond nitrogen-vacancy centers inside cavities. *Phys. Rev. A* **88,** 042323 (2013).
46. Wang, T.-J. & Wang, C. Universal hybrid three-qubit quantum gates assisted by a nitrogen-vacancy center coupled with a whispering-gallery-mode microresonator. *Phys. Rev. A* **90,** 052310 (2014).
47. Luo, M.-X., Li, H.-R. & Wang, X. Teleportation of a controlled-NOT gate for photon and electron-spin qubits assisted by the nitrogen-vacancy center. *Quantum Infor. & Comput*. **15,** 1397–1419 (2015).
48. Luo, M.-X. & Wang, X. Universal remote quantum computation assisted by the Cavity input-output process. *Proc. R. Soc. Lond. A* **471,** 20150274 (2015).
49. Park, Y.-S., Cook, A. K. & Wang, H. Cavity QED with diamond nanocrystals and silica microspheres. *Nano Lett.* **6,** 2075–2079 (2006).
50. Schietinger, S., Schröder, T. & Benson, O. One-by-One coupling of single defect centers in nanodiamonds to high-Q modes of an optical microresonator. *Nano Lett.* **8,** 3911–3915 (2008).
51. Barbour, R. J., Dinyari, K. N. & Wang, H. A composite microcavity of diamond nanopillar and deformed silica microsphere with enhanced evanescent decay length. *Opt. Express* **18,** 18968–18974 (2010).
52. Barclay, P. E., Fu, K. M. C., Santori, C. & Beausoleil, R. G. Chip-based microcavities coupled to nitrogen-vacancy centers in single crystal diamond. *Appl. Phys. Lett*. **95,** 191115 (2009).
53. Fu, K.-M., Barclay, P., Santori, C., Faraon, A. & Beausoleil, R. Low temperature tapered-fiber probing of diamond NV ensembles coupled to GaP microcavities. *New J. Phys.* **13,** 055023 (2011).
54. McCutcheon, M. W. & Loncar, M. Design of a silicon nitride photonic crystal nanocavity with a Quality factor of one million for coupling to a diamond nanocrystal. *Opt. Express* **16,** 19136–19145 (2008).
55. Duan, L.-M. & Kimble, H. J. Scalable photonic quantum computation through cavity-assisted interactions. *Phys. Rev. Lett.* **92,** 127902 (2004).
56. Ren, B. C. & Deng, F. G. Hyper-parallel photonic quantum computation with coupled quantum dots. *Sci. Rep*. **4,** 4623 (2014).
57. Hua, M., Tao, M. J. & Deng, F. G. Universal quantum gates on microwave photons assisted by circuit quantum electrodynamics. *Phys. Rev. A* **90,** 012328 (2014).
58. Hu, C. Y., Young, A., O'Brien, J. L., Munro, W. J. & Rarity, J. G. Giant optical Faraday rotation induced by a single-electron spin in a quantum dot: applications to entangling remote spins via a single photon. *Phys. Rev. B* **78,** 085307 (2008).
59. Bonato, C. *et al.* CNOT and Bell-state analysis in the weak-coupling cavity QED regime. *Phys. Rev. Lett.* **104,** 160503 (2010).
60. Reiserer, A., Kalb, N., Rempe, G. & Ritter, S. A quantum gate between a flying optical photon and a single trapped atom. *Nature* **508,** 237–240 (2014).
61. Wei, H. R. & Long, G. L. Hybrid quantum gates between flying photon and diamond nitrogen-vacancy centers assisted by optical microcavities. *Sci. Rep*. **5,** 12918 (2015).
62. Luo, M.-X. & Wang, X. Parallel photonic quantum computation assisted by quantum dots in one-side optical microcavities. *Sci. Rep*. **4,** 5732 (2014).
63. Luo, M.-X., Deng, Y., Li, H.-R. & Ma, S.-Y. Photonic ququart logic assisted by the cavity-QED system. *Sci. Rep*. **5,** 13255 (2015).
64. Vallone, G., Ceccarelli, R., De Martini, F. & Mataloni, P. Hyperentanglement of two photons in three degrees of freedom. *Phys. Rev. A* **79,** 030301 (2009).
65. Vallone, G., Donati, G., Ceccarelli, R. & Mataloni, P. Six-qubit two-photon hyperentangled cluster states: Characterization and application to quantum computation. *Phys. Rev. A* **81,** 052301 (2010).
66. Manson, N. B., Harrison, J. P. & Sellars, M. J. Nitrogen-vacancy center in diamond: Model of the electronic structure and associated dynamics. *Phys. Rev. B* **74,** 104303 (2006).
67. Walls, D. F. & Milburn, G. J. (ed.) [*Quantum Optics*] [250–350] (Springer-Verlag, Berlin, 1994).
68. Kimble, H. J. Strong interactions of single atoms and photons in cavity QED. *Phys. Scr.* **76,** 127 (1998).
69. Chen, Q., Yang, W. L., Feng, M. & Du, J. F. Entangling separate nitrogen-vacancy centers in a scalable fashion via coupling to microtoroidal resonators. *Phys. Rev. A* **83,** 054305 (2011).

70. Xiao, Y. F. *et al.* Quantum electrodynamics in a whispering-gallery microcavity coated with a polymer nanolayer. *Phys. Rev. A* **81,** 053807 (2010).
71. Luxmoore, I. J. *et al.* Restoring mode degeneracy in H1 photonic crystal cavities by uniaxial strain tuning. *Appl. Phys. Lett.* **100,** 121116 (2012).

Acknowledgements

This work is supported by the National Natural Science Foundation of China (No. 61303039), the Fundamental Research Funds for the Central Universities (No. XDJK2016C043), the Doctoral Program of Higher Education (No. SWU115091), and Science Foundation Ireland (SFI) under the International Strategic Cooperation Award Grant Number SFI/13/ISCA/2845.

Author Contributions

M.-X.L. proposed the theoretical method. M.-X.L. and H.-R.L. wrote the main manuscript text. M.-X.L. and H.L. and X.W. reviewed the manuscript.

Additional Information

Supplementary information accompanies this paper at http://www.nature.com/srep

Competing financial interests: The authors declare no competing financial interests.

How to cite this article: Luo, M.-X. *et al.* Quantum Computation Based on Photons with Three Degrees of Freedom. *Sci. Rep.* **6**, 25977; doi: 10.1038/srep25977 (2016).